INL/JOU-23-71233-Revision-0

Investigating solgel matrix loading capacity toward producing surrogate nuclear explosive debris with realistic composition

January 2024

Justin Teryl Cooper, Mathew S Snow, George Diehl, Tara Mastren, Thomas Vernon Holschuh II, David L Chichester

Changing the World's Energy Future

INL/JOU-23-71233-Revision-0

Investigating solgel matrix loading capacity toward producing surrogate nuclear explosive debris with realistic composition

Justin Teryl Cooper, Mathew S Snow, George Diehl, Tara Mastren, Thomas Vernon Holschuh II, David L Chichester

January 2024

Idaho National Laboratory
Idaho Falls, Idaho 83415

http://www.inl.gov

Prepared for the
U.S. Department of Energy
Under DOE Idaho Operations Office
Contract DE-AC07-05ID14517

Investigating Sol-Gel Matrix Loading Capacity Toward Producing Surrogate Nuclear Explosive Debris with Realistic Composition

Names of authors: George Diehl[1], Justin T. Cooper[2*], Tara Mastren[1], Tommy V. Holschuh[2], David L. Chichester[2], Mathew Snow[2]

Affiliations and addresses of the authors:

[1] Nuclear Engineering Program, University of Utah, 110 Central Campus Dr, Salt Lake City, UT 84112, USA

[2] Idaho National Laboratory, 2351 N. Boulevard Idaho Falls, ID 83415-2805, USA

[*] Corresponding Author: justin.cooper@inl.gov

Investigating Sol-Gel Matrix Loading Capacity Toward Producing Surrogate Nuclear Explosive Debris with Realistic Composition

George Diehl[1], Justin T. Cooper[2*], Tara Mastren[1], Tommy V. Holschuh[2], David L. Chichester[2], Mathew Snow[2]

[1] Nuclear Engineering Program, University of Utah, 110 Central Campus Dr, Salt Lake City, UT 84112, USA
[2] Idaho National Laboratory, 2351 N. Boulevard Idaho Falls, ID 83415-2805, USA
[*] Corresponding Author: justin.cooper@inl.gov

Abstract

Post detonation nuclear forensic materials which resemble the size, color, elemental composition, and radionuclide content of real nuclear debris would be valuable for developing and validating new nuclear forensic techniques. As nuclear fallout types vary significantly, the ability to tailor each of these parameters accurately is desired to produce materials capable of testing analytical methods under a wide array of forensic scenarios. Sol-gel synthesis techniques can provide tunability of size, shape and composition for producing a wide variety of solid nuclear forensics benchmarking materials. The sol-gel process consists of forming a metal oxide material, often silica, through polymerization of a metal-alkoxy precursor. In this work, we characterize the ability to load sol-gel particles with secondary elemental components such as iron, aluminum, and calcium toward producing benchmarking materials approximating the elemental composition of historic nuclear debris from the Nevada National Security Site. We also demonstrate quantitative radionuclide encapsulation toward producing benchmarking materials with controllable radionuclide content. Finally, we employ these techniques to produce nuclear debris benchmarking materials with controllable elemental matrix composition and radionuclide content and compare these samples with the composition of a historic fallout sample previously reported from the Nevada National Security Site.

Keywords: Surrogate nuclear explosive debris, sol-gel, metal loading, nuclear forensics

1. Introduction

Post-detonation nuclear forensic analysis is a key capability for elucidating the origin of a nuclear device, the likelihood of additional devices or threats, and so forth.[1-5] Each of these pieces of information are crucial to decision makers as they determine the national response to a nuclear attack.

A large number of post-detonation nuclear forensic techniques are currently under development worldwide; such approaches include nuclear fallout collections, in-field

analyses and screening techniques, and rigorous analytical laboratory analyses.[5-7] In order to evaluate and optimize new and emerging techniques, nuclear explosive debris that contains realistic particle sizes, colors, elemental compositions, and radiological signatures is needed. As debris from historic nuclear testing no longer contains the radiological activity consistent with a recent detonation, capabilities to synthesize realistic surrogate nuclear explosive debris (SNED) are required.

The complex chemical and physical processes associated with nuclear debris formation make producing SNED a significant challenge. Upon detonation, a nuclear device vaporizes all materials in the immediate surrounding environment. Within milliseconds to seconds the fireball cools to temperatures below the melting point of most of the elemental constituents in the mixture. During this cooling process, different chemical species condense from the vapor phase as a function of their melting points. Differences in elemental and molecular condensation as a function of time results in a heterogeneous distribution of elements in a phenomena known as chemical fractionation[8-13]. During this complex heating and cooling process, a variety of different physical forms of nuclear debris are produced. Larger forms of nuclear debris (often called "fused earth" or "splatter") are produced in the immediate vicinity of near-ground-level detonations. The size of these materials tends to be on the order of centimeters and larger, with a variety of amorphous physical shapes. On the other hand, particles that condense in the air (often called "aerodynamic fallout") tend to be spherical in shape. These particles may range from millimeters to nanometers in size, and thus may be transported many kilometers from the detonation location (with smaller particles generally transported to farther distances).

Historic nuclear detonations in a variety of different environments including the southern United States[14-16], Australia[17], Japan[18] and Russia[19] demonstrate that the bulk composition of nuclear debris of near-ground-level detonations is primarily driven by the composition of the surrounding environment, with silica, calcium, and iron being some of the most common elemental components of land-generated nuclear debris. On the other hand, heterogeneity within individual debris particles is commonly observed from all nuclear tests[14-19], with elemental incorporation driven by their differing chemistries and inclusion of different initial materials into the final debris[12,14,20,21]. Nevertheless, as the surrounding environment can vary substantially from different environments around the globe, the bulk composition of nuclear debris can be drastically different between different events. The extreme differences in nuclear debris composition requires the capability to tailor synthetic SNED to a wide variety of elemental compositions and radionuclide contents with a high degree of reproducibility.

Sol-gel synthesis techniques for SNED synthesis have previously been explored and have demonstrated the ability to encapsulate radionuclides for use in post-detonation nuclear forensics applications. Specifically, radionuclides such as ^{82}Br from activated KBr were incorporated as into sol-gel glass as a surrogate for ^{137}CsCl.[22] Fission products have also been incorporated into sol-gel glasses through preliminary doping of the glass with HEU followed by neutron irradiation[23], as well as by solidification of previously prepared fission product solutions[24].

In this study, the elemental loading capacity of sol-gel particles was investigated to characterize the ability to use the sol-gel method to produce SNED with a wide variety of elemental compositions. The loading capacity for stable sodium, calcium, iron, and aluminum nitrates were chosen for investigation in this work as these elements are likely

to comprise nuclear debris from a variety of environments, including historic nuclear weapons testing debris collected from the Nevada National Security Site (NNSS).[15,25-27] Systematic studies of single, binary, and quaternary component incorporation within sol-gels were performed in this work. Physical changes in the SNED particles as a function of stable element loading were monitored using optical microscopy and scanning electron microscopy (SEM). Energy dispersive X-ray spectroscopy (EDS) was also used to track the spatial distribution and stable element incorporation within particles as a function of the stable element concentration in the sol-gel precursor solution. Finally, we report the production of SNED that mirrors the elemental composition of the average composition in the Earth's crust, as well as debris that contains the matrix composition and short-lived fission product content consistent with generic historic nuclear weapons test debris from the NNSS.

2. Experimental

2.1 Reagents

Tetraethyl orthosilicate (TEOS), 98%, was purchased from ACROS Organics. Ethyl alcohol (200 proof HPLC grade), aluminum nitrate nonahydrate (98%, ACS reagent grade), iron (III) nitrate nonahydrate (98%, ACS reagent grade), calcium nitrate tetrahydrate (99%, ACS reagent grade), calcium chloride dihydrate (crystals, ACS grade), and sodium chloride (molecular biology grade) were purchased from Sigma Aldrich. Nitric acid (optima grade) and sodium nitrate (certified ACS crystal) were purchased from ThermoFisher Scientific. Iron (III) chloride hexahydrate (97-102%, ACS grade) was purchased from Alfa Aesar.

2.2 Particle Synthesis

Sol-gel particles were synthesized using an acid-catalyzed method. Briefly, separate aliquots of sodium, calcium, aluminum, and iron nitrate salts were dissolved in 3 M nitric acid. Aliquots of metal-acid solutions were then combined with TEOS and ethanol in a 3.2:3:20 ratio of TEOS:ethanol:3 M HNO_3, respectively. The amount of metal within each batch of particles was systematically varied from 2.5-80 mol % relative to the combined moles of Si from the TEOS and the added metal. Multi-element doped particles were also produced from 5-75 mol %, representing the total added metal relative to the combined moles of Si and the metals, with each metal added in equal molar amounts. After combining, each sample was agitated by hand for 2 minutes, following which 1-10 µL droplets were pipetted onto hydrophobic sheets and air dried for a minimum of 18 hours. Samples were then gently scraped from the sheets and subsequently analyzed.

2.3 Sol-gel Thermal Treatment

To investigate the impact of annealing upon the elemental composition at the micron scale within individual particles, a select number of samples containing stable elements were placed in a muffle furnace at 600°C for 2 hours, with the temperature ramped from ambient at a rate of 10°C/min. Following heat treatment, the oven was shut

off and the particles were allowed to gradually return to ambient temperature inside the oven over a 12-hour period prior to removal and subsequent analysis.

2.4 Nonradioactive SNED Production

To demonstrate the capability to match a generic crustal metal abundance, a sol-gel solution was doped with appropriate amounts of aluminum, iron, calcium, and sodium nitrate to produce particles with a weight percent of each element that approximates the average composition of the Earth's crust (which is similar to plagioclase and alkali feldspar).[28] Following vitrification using the approach described in sections 2.2 and 2.3 above, particles from this sample were analyzed for elemental composition via scanning electron microscopy with x-ray energy dispersive spectroscopy (SEM/EDS). Upon success, a second series of samples targeting reproducing the metal abundance reported for historic nuclear weapons debris from the NNSS[15] were produced using this same approach.

2.5 Nevada National Security Site SNED Production

Realistic SNED must contain both the major stable element composition of the environment in which the detonation occurred and short-lived radioactive fission products present within a few hours of a recent fission event. To demonstrate the ability to meet these requirements, a sample containing both the major elemental composition reported for debris from historic nuclear weapons tests at the NNSS and short-lived fission products was synthesized.

Fission products were produced via the photofission process. A 1-gram depleted uranium target was irradiated using 38 MeV end-point bremsstrahlung photons produced at the Idaho State University's high-power S-band electron linear accelerator. Following irradiation and overnight cooling, the target was shipped to Idaho National Laboratory where the depleted uranium was dissolved and the uranium was removed using a UTEVA column separation. An aliquot of the fission product fraction, consisting of 1.16×10^{13} total fissions (based on ^{99}Mo) was obtained and added to an acid solution containing Al, Fe, Ca, and Na at concentrations consistent with those reported for historic NNSS debris [10]. Solid particles were then synthesized according to the procedure reported in sections 2.2 and 2.3 above. Following synthesis, particles were analyzed via SEM/EDS and gamma spectrometry.

2.6 Microscopy

Following vitrification, particles were transferred to carbon SEM tape adhered to SEM stub mounts. SEM stub mounts were then transferred into a JEOL JCM-7000 Benchtop SEM for SEM and EDS analyses. EDS analysis was done with the following SEM settings; signal: BED-S, landing voltage: 15 kV, probe current mode: high-pc, vacuum mode: high vac. For EDS maps, the EDS was set to auto-detect. For point analysis,

the standardless quantitative method was used, where a ZAF (atomic number, absorption, fluorescence) correction is applied using a standard spectrum pre-registered in the JEOL analysis software. All analyses were performed without a standard with the result type set to metal. EDS quantitation is expressed in atom % relative to all detected atoms. This is in contrast to the loading mol % which is expressed relative to the moles of Si and added metal in the original precursor solution.

For particle size measurements, particles from each sample were placed in a polystyrene petri dish (Fisher Scientific) and analyzed using a ZEISS SteREO Discovery V12 optical microscope. Microscope calibrations were performed using a 0.1 mm resolution microscope calibration slide (Fisher Scientific).

2.6 Gamma Spectrometry

For radioactive SNED samples, the fission products were quantified using an Ortec IDM-200-V High Purity Germanium gamma spectrometer (HPGe). Detector efficiency curves were constructed through the use of calibration sources (^{137}Cs, ^{60}Co, and ^{152}Eu) at 10, 20, and 50 cm. Simulations were then performed to extrapolate the detector efficiency curves to the specific source geometry and measurement distance used. Samples were placed at 200 cm from the face of the detector and measured for 14 h.

3. Results and Discussion

3.1 Particle Size

The ability to tailor the particle size of SNED is important to mimic the fallout size variation found at various distances from ground zero.

Figure SI-1 shows the particle size of blank sol-gel particles as a function of the volume of the sol-gel precursor droplet. Blank sol-gel particles have a high degree of size tunability with the particles' size being linearly dependent on the volume of the sol-gel precursor droplet deposited (and thus the number of moles of TEOS per droplet).

The addition of stable element dopant to the sol-gel, shown in Figure 1, results in several interesting trends. The first region of interest is the region from 0-20 mol %, where the trends for Na and Ca glasses result in shallowly sloped lines (Ca) or curves (Na) as opposed to the steeper sloped linear trends observed for higher valent Fe and Al. At these concentrations several phenomena are likely occurring.

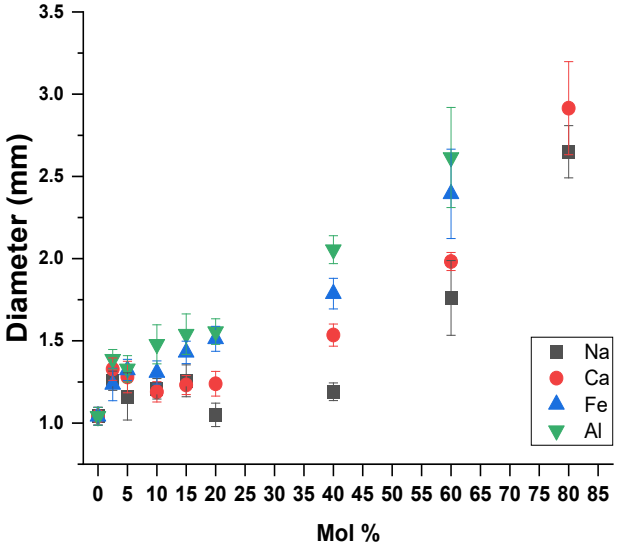

Figure 1. The diameter of the flat, smooth side of the particles as a function of metal mol %. Error bars represent a standard deviation in particles measured ($6 \leq n \geq 22$).

As the tetraethyl orthosilicate transitions from solution to sol-gel to glass, the addition of metal ions likely impacts the resulting silicate condensation and hydrolysis reactions, resulting in changes to the internal cross linking and thus the density of the final glass produced. These alterations are almost certainly dependent on several factors including the ionic charge and the size of the metal ion. Observations to this effect have been made in the literature previously, including inhibition of densification of sol-gels as a function of the multivalency of the dopant cations, [29] and an increase in the specific surface area of loaded versus blank sol-gels via nitrogen adsorption analysis.[30,31] As the specific mechanisms and structural changes resulting from metal additions to sol-gels has not yet been rigorously characterized in the literature, such a study in the future is likely warranted. The second region of interest is the range beyond 20 mol % metal ion concentrations. At these concentrations a linear increase in size is observed as a function of the metal concentration for all metal cations. As is shown in the following sections, this linearity is likely due primarily to the increasing mass of metal ion added and not a complex structural phenomenon. In other words, at concentrations above 20 mol % the total mass of metal ion exceeds the quantity able to be incorporated within the silicate structure. At higher metal concentration (50-80 mol %) the structural integrity of the particles also became increasingly compromised; for example, at 80 mol %, Al and Fe particles did not dry into hemispherical particles, rather they dried into shattered pieces (Figure 2), while Na and Ca particles were likewise extremely brittle.

3.2 Optical Microscopy

Optical microscopy showed that the blank sol-gel particles were hemispherical and translucent (Figure S2). These observations are consistent with expectations for acid catalyzed sol-gel glasses due to the predominance of condensation reactions over hydrolysis reactions for acid catalyzed glasses, as opposed to the more optically opaque structures produced via base catalyzed glasses where hydrolysis reactions are preferred.[32]

Figure 2 shows optical microscope pictures of sol-gel particles as a function of stable element loading. All sol-gel particles maintained their translucent nature at metal loading concentrations below 20 mol %. Between 20 and 40 mol %, a noticeable increase in opacity is observed. Sodium, calcium, and aluminum loaded particles gradually became whiter, consistent with the color of their respective nitrate salts or potentially their solid oxide form. With Fe, the color was noticeable at 10 mol % concentrations, gradually transitioning from a light yellow to a dark orange (Figure 2). The Fe coloration points to the likely formation of Fe(III) oxide following the room temperature decomposition of the nitric acid.

The increased opacity seems to stem from loaded salt or oxide precipitate depositing on the exterior and interior pore surfaces of the particles (as demonstrated with later SEM/EDS

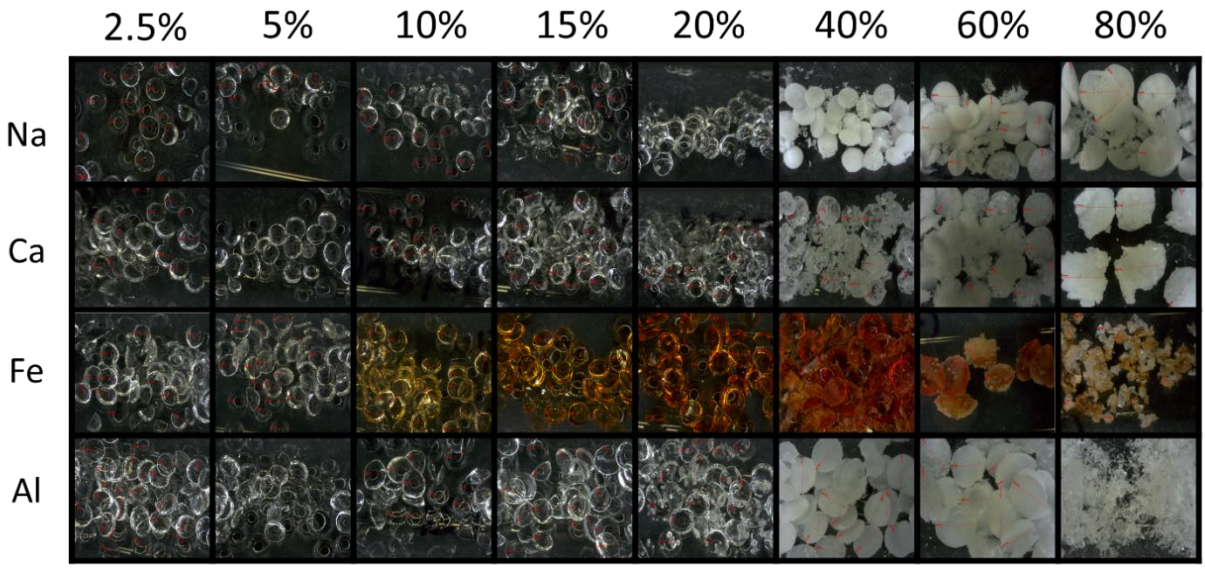

Figure 2. Optical microscopy image of synthesized sol-gel SNED as a function of metal loading.

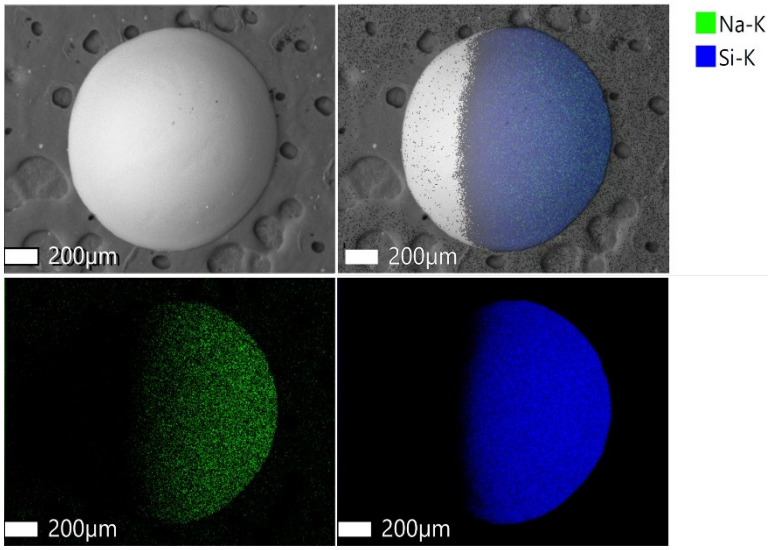

Figure 3. Five mol % Na doped sol-gel particle. (Top left) SEM image. (Top right) EDS map of Na and Si distribution in sol-gel particle. (Bottom left and right) EDS map of Na distribution. (Bottom right) EDS map of Si distribution.

analyses), with the precipitate quantity increasing with the mole percent of the metal. This implies that a limit to the incorporation of the stable metal salts in the interior of the particles (when synthesized under the conditions of this experiment) is reached at roughly 20 mol % of the metal, with any further increases in metal salt in the initial sol-gel solution simply resulting in precipitate formation on the particle surface. Multi-element loaded particles showed a similar trend in color and opacity to their single-element loaded counterparts, with particles remaining translucent until surpassing a total loading level of 20 mol %, after which precipitate features were seen forming on the surface (Figures S3 & S4). Not surprisingly, the color of the particles seemed to be dominated by the reddish Fe component when present as opposed to the lighter colored Na, Ca and Al salts.

3.3 SEM and EDS Analysis of Blank and Single Metal Sol-Gel Samples

SEM analysis of blank glasses showed a smooth surface at the micron scale. EDS analyses of the surfaces of these blank glasses detected only Si and O which were homogenously distributed throughout the blank particles (Figure S2). EDS did not detect nitrogen from nitric acid, likely due to the appreciable decomposition and/or evaporation rate of nitric acid.[33]

SEM-EDS analyses also shed insights into the surface topography and elemental distribution of the loaded sol-gel particles. Similar trends were observed between all stable elements in this work. To simplify the discussion, sodium nitrate doped particles are described in detail in this section, with the data for other elements provided in the Supporting Information Section (see Figures S5, S6 and Table S1). As shown in Figure 3, particles with low amounts of stable metal added (< ~20%) were predominantly smooth, with the loaded element being homogenously distributed across the particle and co-located

with the Si from the silica sol-gel. As the loading level increased, rough features were observed forming on each particle's surface (Figure S5).

Elemental analysis of the surface features produced at stable element loading concentrations above 15-20% showed high concentrations of the metal with little Si present (Figure 4). The abrupt decrease in detected Si on the surface of particles at 15-20 mol %, correlated with an increase in Na, is a clear indication of a change in the chemical composition of surface versus interior at this concentration. Figure 4 also shows an SEM backscatter image, and EDS map of a representative sol-gel particle fragment loaded at 40 mol % with $Na(NO_3)$. The SEM image shows a topologically rough shell surrounding a smoother interior core. The EDS map shows that the rough shell is predominately comprised of Na and N, indicating that it is likely a $Na(NO_3)$ precipitate, while the smooth interior core is predominately Si with fairly evenly distributed Na and N as minor components.

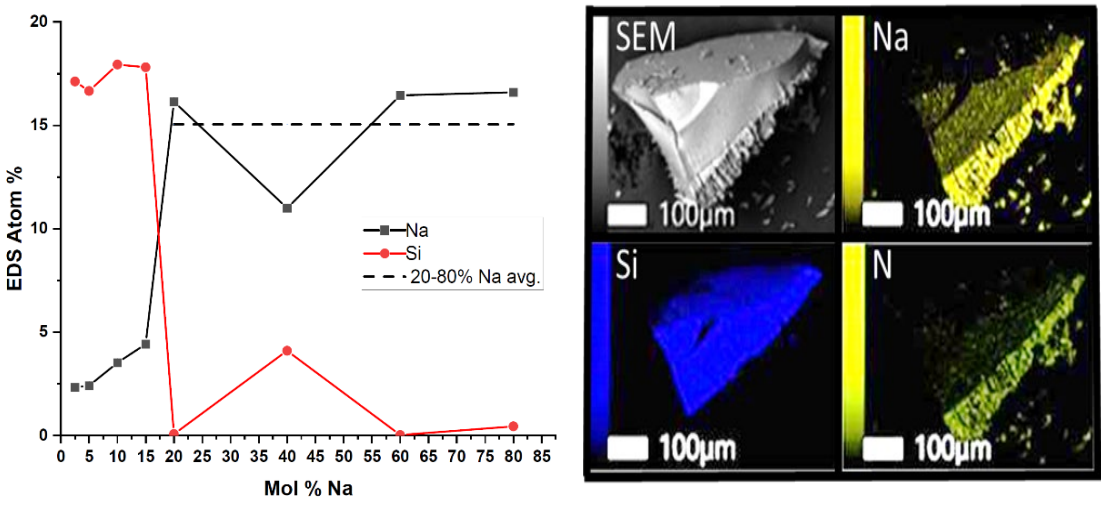

Figure 2. (Left) EDS measured atom % Na and Si on the surface of particles as a function of mol % doped Na. (Right) SEM and EDS analysis of 40% Na doped particle, showing the smooth silica interior with an exterior shell enriched in $Na(NO_3)$.

EDS analysis results of the fractured $NaNO_3$ doped sol-gel particle's surface and interior (Figure 4), are summarized in Table 1 (note that EDS quantitation is expressed in atom % relative to all detected atoms while loading mol % Na is relative to mols Si and added metal in the original solution). The amount of Na found in the Si interior for a 40 mol % loaded particle was measured to be approximately 4 atom %. This is roughly equivalent to the quantity measured for a particle loaded to the 15 mol % Na level (see Figure 4). This further lends credence to the hypothesis that the sol-gel silica reaches an Na incorporation limit at approximately the 15 mol % level and any further increase in loading level results in precipitate formation on the surface of the particle.

Table 1. Point analysis of 40 and 15 mol % Na loaded particles with EDS. Points were analyzed on the smooth interior or on the surface features for the 40 mol % particles and as an averaged over the entirety of the particle for the 15 mol %. (Detected C, O and N not shown).

Location	Si (atom %)	Na (atom %)
40 mol % Na (particle Interior)	16 ± 4.6	4.0 ± 1.7
40 mol % Na (surface feature)	0.0 ± 0.0	14.0 ± 3.2
15 mol % Na (whole particle aggregate)	17.81 ± 0.04	4.42 ± 0.03

3.3 SEM and EDS Analysis of Multi-Element Sol-Gel Samples

As with the single element loaded particles, multi-element loaded particles showed a continuous distribution of metals and Si across the particle for metal loading levels below 20 % (Figure S7). Additionally, EDS mapping showed that at higher loading levels, surface precipitate features were enriched in the loaded elements. However, surface features were found to be concentrated in a single loaded component rather than multiple loaded elements simultaneously (Figure 5). As the dopant levels increase, precipitate features dominated the surface and the metals remained largely phase segregated with little to no Si present. Where the interior core of the particle was exposed (and thus the surface of particles were easily interrogatable by EDS), Si was the dominant composition with much lower metal levels relative to the surface shell.

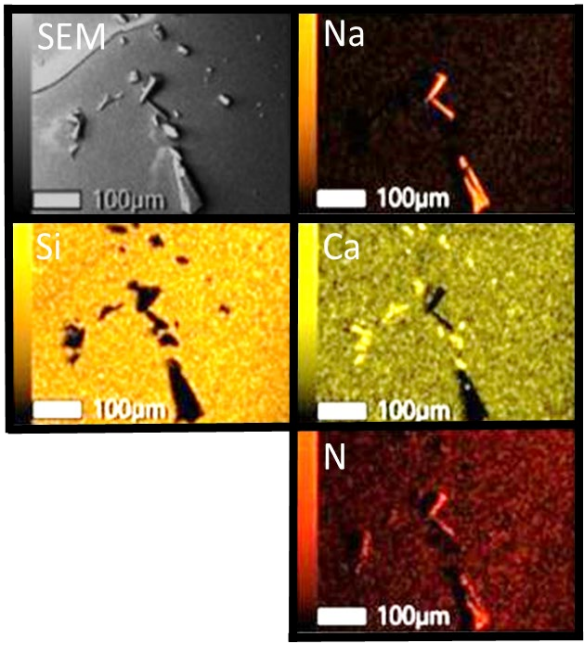

Figure 3. Zoomed in EDS analysis of surface features on a Na + Ca sol-gel particle. 20 total mol %.

A quaternary loaded sol-gel was also produced where Na, Ca, Fe, and Al nitrate salts were all added to the sol-gel particles together. The behavior of these were similar to

that of the singly and doubly loaded particles, where at high loading levels rough features enriched in the loaded elements covered a smooth Si rich interior. (Figure 6). As in the binary mixture, EDS analysis showed phase segregation occurring in the elemental distribution of surface precipitates. Ca and Fe seemed to have lower propensities to form highly enriched surface features when compared to Na and Al. This is evident from the intensity scale in Figure 6 showing highly enriched surface features for Na and Al relative to the concentration co-located with the Si background, while the surface features for Ca and Fe are much lower in concentration relative to its Si core concentration. The relative distributions of each dopant do not seem to trend with any discernable physical property such as ionic radius, ionic valency, charge density, or water solubility, though additional analyses are likely needed to definitively evaluate these correlations statistically. Similar difficulty in discerning the mechanism of the association of stable-elements with the silica matrix has been found in the literature [31,30] and this is recommended to be the subject of future investigations.

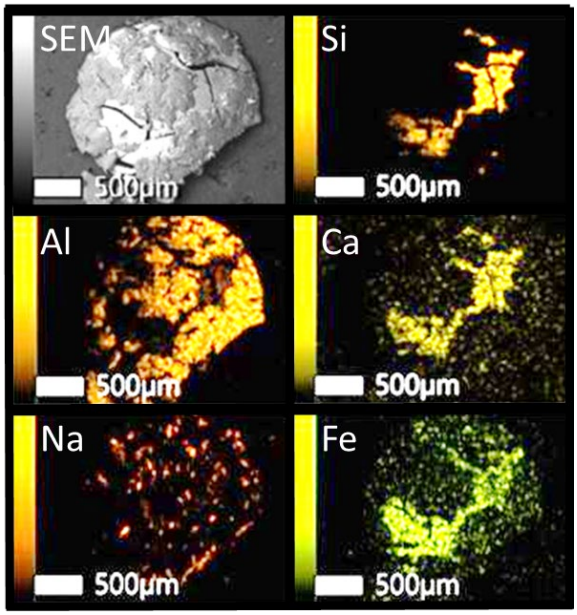

Figure 6. Right: EDS analysis of 40% doped particle (10% for Na, Ca, Fe, and Al each).

3.4 Thermal Treatment

Thermal treatment of sol-gel is standard practice to drive off excess water and to strengthen the gel by promoting cross-linking and conversion of remaining silanol groups to siloxane bonds. A rigorous investigation of the effects of thermal treatment on the distribution of loaded elements within sol-gel particles is the subject of future publication, however here the effect of a standard sol-gel thermal treatment for particles of this nature (600 °C for 2 hr) was explored briefly.

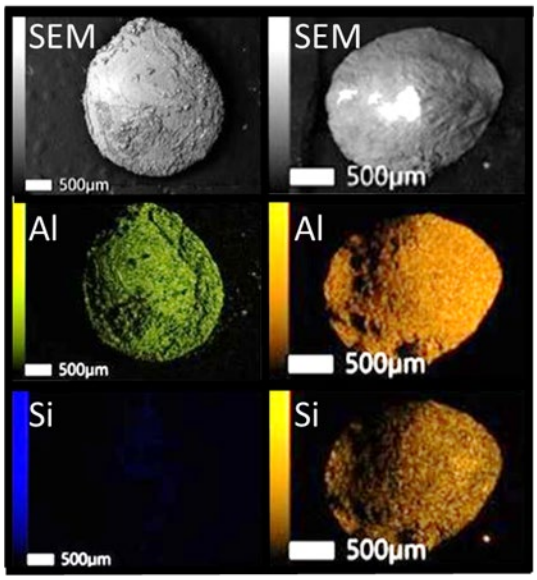

Figure 7. EDS analysis of a particle doped with 60% Al before (left) and after (right) annealing.

Thermal treatment of particles with low metal loading content had very little effect on their appearance observable by SEM or metal distribution by EDS analysis. However, at higher loading levels, where an enriched surface shell was present, thermal treatment resulted in the disappearance of most of these features (Figure 7). It is unlikely that metal was lost from the particles as the temperature used to treat the particles was well below the melting points for each element. Rather, the data supports the hypothesis that during heat treatment of the particles at higher temperatures the glass softens sufficiently to enable re-ordering of the silicate structure and reincorporation of the metals within the structure. In other words, it appears that it may be feasible to incorporate metal concentrations higher than 15-20 mol % if a thermal treatment is performed. Additional, focused investigations on the structural changes that occur with annealing are needed to verify this hypothesis and have been included in future funding proposals. Nitrogen was found to be completely removed in all thermally treated particles, likely to the decomposition of nitrate and its loss as NO_2.

3.5 Nevada Test Site Matrix Sol-gel Surrogate Nuclear Debris

The ultimate application for this work was to produce sol-gel based SNED with stable elemental loading levels simulating that of actual nuclear fallout from specific environments. With that goal in mind, Table 2 shows the elemental composition of a glass containing the stable elemental composition reported for average earth crustal abundance. Specifically, this composition was similar to plagioclase feldspar, the major components of the earth's crust.[28] In general, good agreement between the targeted elemental composition and the composition in the crustal abundance glass sample is observed. Importantly, the approximate total mol % of dopant for this sample is 18% which is approximately the point where we have found surface precipitates begin to form.

Table 2. Results of sol-gel doped with constituents resembling the composition of earth's crust.

Element	Target Wt. %	Wt. %	Mol % to SiO_2
Al	6.69	6.6 ± 0.1	8.93
Fe	4.47	4.0 ± 0.1	4.94
Ca	2.82	2.0 ± 0.1	2.71
Na	5.24	5.0 ± 0.1	10.03

After thermal treatment, particles from the crustal abundance sample took on a reddish-brown color, suggesting the transition of the iron nitrate to iron oxide (Figure S8). Furthermore, no nitrogen was detected via EDS indicating the conversion of all or most of the nitrate dopants to their oxide forms. At first glance, the SEM and EDS analysis show a mostly smooth particle with dopants distributed across the entirety of the particle (Figure 8).

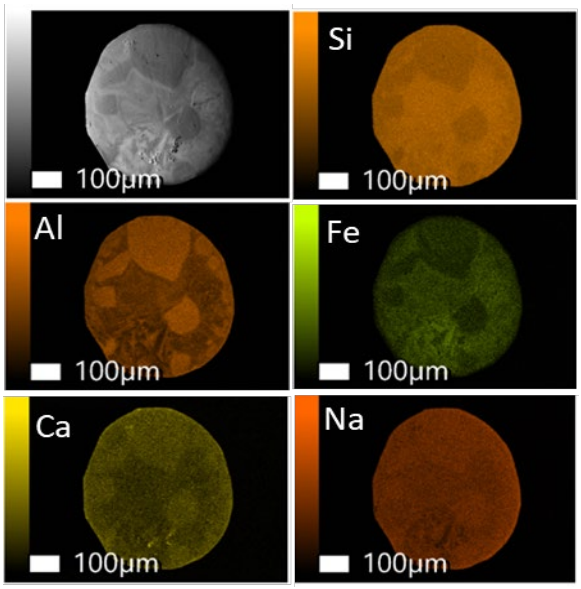

Figure 8. SEM and EDS of soil matrix sol-gel particles.

However, upon closer inspection, there is a small amount of heterogeneity in the distribution of each element with what appears to be surface precipitate shells that are enriched in certain dopants over a smooth shell containing Si. Aluminum has a heterogenous distribution, appearing with a higher concentration in the precipitate shell, than co-located with the Si. Calcium appears to mirror the behavior of Al, but with a less pronounced difference in concentration between the Si core and shell as with Al. Fe, on the other hand, skews toward higher relative concentrations, co-localized with the silica core regions. The behavior of Al and Fe relative to Si are consistent with the previous multi-element doped particles, but Ca's behavior differs as Figure 8 shows Ca co-located with Fe and Si.

The observation of heterogeneous distribution of metals within sol-gel samples is consistent with observations made on real aerodynamic nuclear debris particles.[15,26] For example, Weisz et al. analyzed agglomerated fallout glasses from a uranium-fueled, near surface nuclear test and found the interior of the particles to vary in terms of chemical

homogeneity; some being relatively homogenous, and other distinctly heterogenous with concentrated regions of metal, and even nearly pure pockets of SiO_2. Additionally, they found that Fe, Ca, Mg, Mn, and ^{235}U were consistently enriched in the interface layer between particles relative to the particles' interiors, while Ti and Al were consistently depleted. On the other hand, the behavior of Na and K differed between particles, being enriched in the interface in 5 and 3 of the 9 particles studied, respectively. While the behavior of specific elements may be challenging to match between SNED and real debris, the data in this work indicates that SNED synthesized via the sol-gel method can be tailored to show either a high degree of metal homogeneity or heterogeneity throughout the particle, which may be beneficial in simulating the microstructural composition observed in aerodynamic nuclear debris.

Finally, SNED was produced from a quaternary loaded silica sol-gel which incorporated major elemental matrix components from documented NNSS nuclear debris. The targeted and measured weight % of each element along with a comparison to NNSS elemental compositions are shown in Table 3.

Table 3. Target and measured wt% of NNSS like radiological sol-gel surrogate nuclear debris.

Element	Target NNSS Wt. %	Measured Wt. %
Al	7.28	9.0 ± 0.2
Fe	2.06	2.0 ± 0.2
Ca	1.34	1.4 ± 0.1
Mg	0.328	0.33 ± 0.04

The measured composition of the NNSS matrix debris correlated closely with the targeted documented composition of existing NNSS debris.[15,26,25] All metal components were measured to be within 4% of the target value with aluminum as the outlier yet still only being a factor 1.2x high. The spatial distribution of the loaded elements agreed with our previous observations of the quaternary loaded and soil matrix particles (Figure S9).

These particles were additionally doped with fission product radionuclides with a target level of approximately 1.16×10^{13} fissions per gram. The radionuclide content of the dopant solution and particles was analyzed via gamma spectrometry and the gamma spectrum is shown in Figure 9 (See Table S2 for radionuclides).

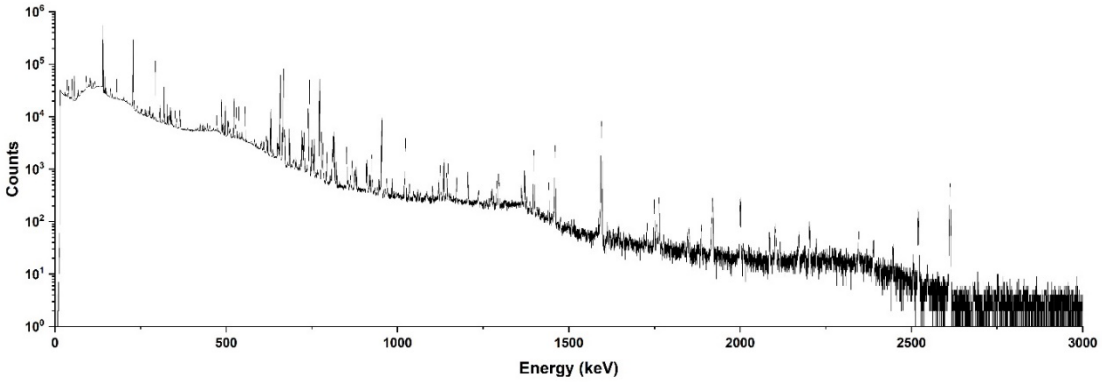

Figure 9. Gamma Spectrum showing fallout relevant fission product incorporation into sol-gel SNED.

Gamma spectroscopy analysis confirmed the quantitative encapsulation of the fission products resulting in an encapsulation of $1.16 \pm 0.04 \times 10^{13}$ fissions per gram of sol-gel and a measured contact dose rate of approximately 350 mrem/h/g. This radionuclide content and dose rate approaches what is expected from actual aerodynamic fallout collected following a detonation and to our knowledge is the first sol-gel production of aerodynamic surrogate nuclear debris with realistic radionuclide content, dose rate and elemental matrix composition.

4. Conclusion

The loading capacity of silica sol-gel particles loaded with the nitrate salts of Al, Fe, Na and Ca was investigated via SEM and EDS analysis. At concentrations below 20 mol % metal ions are found to be homogeneously distributed throughout particles. Upon higher loading levels surface precipitation of the metals is observed, with thermal treatment found able to drive metals back into the matrix and increase loading concentrations above 20 mol %. Binary- and quaternary metal study results agreed with those of single elements, in that quantitative inclusion of the elements within particles at concentrations < 20 mol % total metal loading is observed, with the ability to drive the metals toward either homogeneous or heterogeneous inclusion within particles based upon the specific chemical/thermal process employed during synthesis. As heterogeneous distribution of elements is routinely observed in real debris, these observations suggest sol-gel synthesized SNED may potentially be employed and tuned to simulate both the bulk and micro composition of nuclear debris for certain conditions and scenarios.

Finally, the ability to produce realistic SNED samples was demonstrated via production of a sample containing the major elemental composition reported for historic nuclear debris from a near surface nuclear test at the NNSS. In addition to replicating the major elemental composition of this test, the SNED sample produced in this work

contained a total of 1.16 x 10^{13} total fissions, with the fission product composition consistent with unfractionated photofission product distribution at 48 hours following the original fission event. To our knowledge this represents the first study to simulate the fission product content, dose rate, and elemental matrix composition simultaneously for real debris collected shortly after a nuclear event.

5. Acknowledgements

This work was funded by the Office of Defense Nuclear Nonproliferation Research and Development within the U.S. Department of Energy's National Nuclear Security Administration.

6. Confict of Interest Statement

There are no known conflicts of interest to report associated with this work.

7. Data Availability Statement

No material or data has been gathered from living or dead patients in conjunction with this work.

8. References

1. Dunlop W, Smith H (2006) Post-Detonation Nuclear Forensics. Arms Control Today 36:9
2. Bellucci J, Simonetti A (2012) Nuclear forensics: searching for nuclear device debris in trinitite-hosted inclusions. J Radioanal Nucl Chem 293:313-319
3. Bellucci JJ, Simonetti A, Wallace C, Koeman EC, Burns PC (2013) Isotopic Fingerprinting of the World's First Nuclear Device Using Post-Detonation Materials. Anal Chem 85:4195-4198
4. Davis J (2014) Post detonation nuclear forensics. AIP Conference Proceedings 1596:206-209
5. Stratz SA, Gill JA, Auxier II JD, Hall HL (2016) Modern Advancements in Post-Detonation Nuclear Forensic Analysis. International Journal of Nuclear Security 2:6
6. Jodoin VJ, Lee RW, Peplow DE, Lefebvre JP (2011) Application of the ORIGEN fallout analysis tool and the DELFIC fallout planning tool to national technical nuclear forensics. Proceedings of 11th Emergency Preparedness & Response Conference, Knoxville, TN August 7-10, 2011
7. Cassata W, Gharibyan N, Isselhardt B, Matzel J, Parsons-Davis T (2022) Nuclear Forensics. LLNL-TR-834729. Lawrence Livermore National Lab.(LLNL), Livermore, CA (United States)
8. Freiling E (1961) Radionuclide fractionation in bomb debris. Science 133:1991-1998

9. Freiling EC (1963) Theoretical basis for logarithmic correlations of fractionated radionuclide compositions. Science 139:1058-1059
10. Freiling E (1963) Fractionation 3. Estimation of Degree of Fractionation and Radionuclide Partition for Nuclear Debris. USNRDL-TR-680; AD-423725. NAVAL RADIOLOGICAL DEFENSE LAB, San Fransisco, CA
11. Freiling EC, Crocker GR, Adams CE Nuclear debris formation. In: Radioactive fallout from nuclear weapons tests. Proceedings of an USAEC Conference. Washington, DC: US Atomic Energy Commission, 1965. pp 1-41
12. Dardenne YM, Parker WE, Knight KB (2020) Chemical Fractionation is not a Constant: Revisiting Bomb Vapor Chemistry. LLNL-JRNL-814770. Lawrence Livermore National Lab.(LLNL), Livermore, CA (United States)
13. Izrael YA (2002) Radioactive Fallout After Nuclear Explosions and Accidents. 1 edn. Elsevier, Kidlington, Oxford, UK
14. Bonamici CE, Kinman WS, Fournelle JH, Zimmer MM, Pollington AD, Rector KD (2017) A geochemical approach to constraining the formation of glassy fallout debris from nuclear tests. Contrib Mineral Petrol 172:1-23
15. Weisz DG, Jacobsen B, Marks NE, Knight KB, Isselhardt BH, Matzel JE, Weber PK, Prussin SG, Hutcheon ID (2017) Deposition of vaporized species onto glassy fallout from a near-surface nuclear test. Geochim Cosmochim Acta 201:410-426
16. Bellucci JJ, Simonetti A, Koeman EC, Wallace C, Burns PC (2014) A detailed geochemical investigation of post-nuclear detonation trinitite glass at high spatial resolution: Delineating anthropogenic vs. natural components. Chem Geol 365:69-86
17. Johansen MP, Child DP, Collins R, Cook M, Davis J, Hotchkis MA, Howard DL, Howell N, Ikeda-Ohno A, Young E (2022) Radioactive particles from a range of past nuclear events: challenges posed by highly varied structure and composition. Sci Total Environ 842:156755
18. Wannier MM, de Urreiztieta M, Wenk H-R, Stan CV, Tamura N, Yue B (2019) Fallout melt debris and aerodynamically-shaped glasses in beach sands of Hiroshima Bay, Japan. Anthropocene 25:100196
19. Lukashenko S, Kabdyrakova A, Lind O, Gorlachev I, Kunduzbayeva A, Kvochkina T, Janssens K, De Nolf W, Yakovenko Y, Salbu B (2020) Radioactive particles released from different sources in the Semipalatinsk Test Site. Journal of environmental radioactivity 216:106160
20. Cassata W, Prussin S, Knight K, Hutcheon I, Isselhardt B, Renne P (2014) When the dust settles: stable xenon isotope constraints on the formation of nuclear fallout. Journal of environmental radioactivity 137:88-95
21. Bonamici CE, Hervig RL, Kinman WS (2017) Tracking radionuclide fractionation in the first atomic explosion using stable elements. Anal Chem 89:9877-9883
22. Carney K, Finck M, McGrath C, Brush B, Jansen D, Dry D, Brooks G, Chamberlain D (2013) The development of radioactive sample surrogates for training and exercises. J Radioanal Nucl Chem 296:769-773
23. Carney KP, Finck MR, McGrath CA, Martin LR, Lewis RR (2014) The development of radioactive glass surrogates for fallout debris. J Radioanal Nucl Chem 299:363-372
24. Lusk R, Meirers J, Bucher B, Forbush S, Carney K, Chichester DL, Snow M (2023) Retention of Radionuclides in Sol-gel Surrogate Nuclear Explosive Debris. J Radioanal Nucl Chem In Press
25. Weisz DG, Jacobsen B, Marks NE, Knight KB, Isselhardt BH, Matzel JE (2018) Diffusive mass transport in agglomerated glassy fallout from a near-surface nuclear test. Geochim Cosmochim Acta 223:377-388

26. Lewis L, Knight K, Matzel J, Prussin S, Zimmer M, Kinman W, Ryerson F, Hutcheon I (2015) Spatially-resolved analyses of aerodynamic fallout from a uranium-fueled nuclear test. Journal of environmental radioactivity 148:183-195
27. Fahey AJ, Zeissler CJ, Newbury DE, Davis J, Lindstrom RM (2010) Postdetonation nuclear debris for attribution. Proceedings of the National Academy of Sciences 107:20207-20212
28. Shapley P (2010) The Earth's Crust. http://butane.chem.uiuc.edu/pshapley/Environmental/L26/1.html. Accessed February 22 2022
29. Nedelec J-M, Courtheoux L, Jallot E, Kinowski C, Lao J, Laquerriere P, Mansuy C, Renaudin G, Turrell S (2009) ChemInform Abstract: Materials Doping Through Sol—Gel Chemistry: A Little Something Can Make a Big Difference. ChemInform 40
30. Johnson MFL (1990) Surface area stability of aluminas. J Catal 123:245-259
31. Rossignol S, Kappenstein C (2001) Effect of doping elements on the thermal stability of transition alumina. Int J Inorg Mater 3:51-58
32. Buckley AM, Greenblatt M (1994) The Sol-Gel Preparation of Silica Gels. J Chem Educ 71:599
33. Robertson GD, Mason DM, Corcoran WH (1955) The Kinetics of the Thermal Decomposition of Nitric Acid in the Liquid Phase. The Journal of Physical Chemistry 59:683-690

Supplementary Information

Investigating Sol-Gel Matrix Loading Capacity Toward Producing Surrogate Nuclear Explosive Debris with Realistic Composition

George Diehl[1], Justin T. Cooper[2*], Tara Mastren[1], Tommy V. Holschuh[2], David L. Chichester[2], Mathew Snow[2]

[1] Nuclear Engineering Program, University of Utah, 110 Central Campus Dr, Salt Lake City, UT 84112, USA

[2] Idaho National Laboratory, 2351 N. Boulevard Idaho Falls, ID 83415-2805, USA

[*] Corresponding Author: justin.cooper@inl.gov

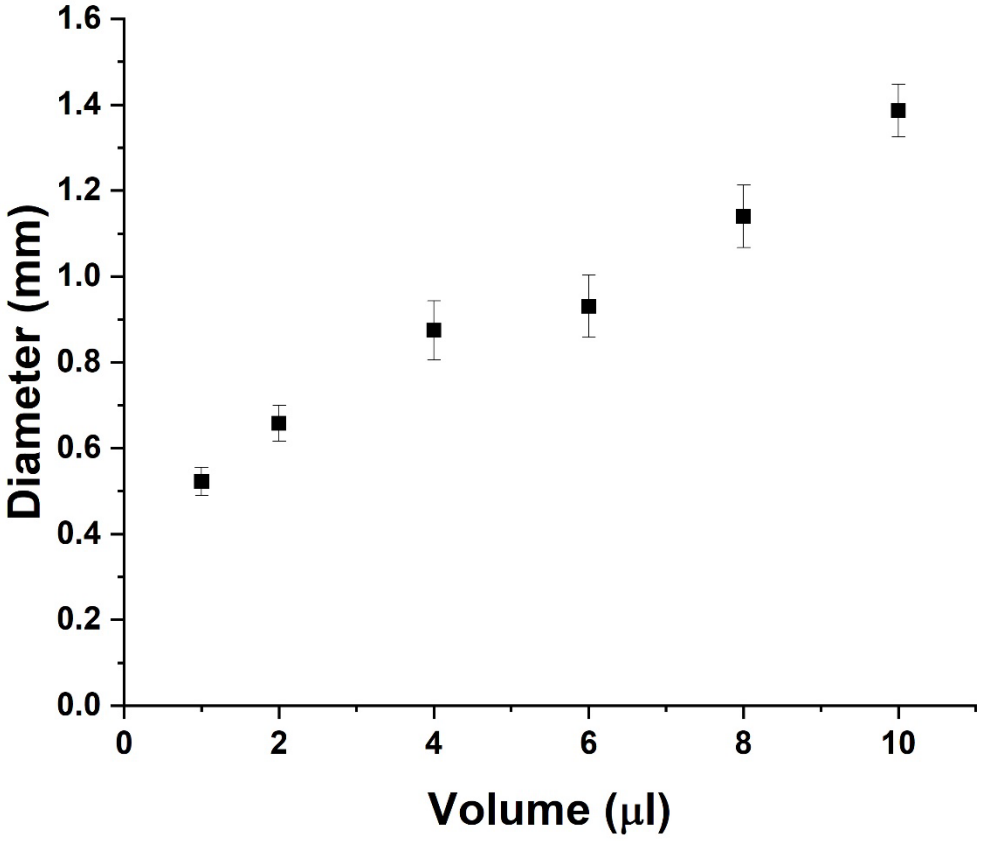

Figure S1. Diameter of non-doped sol-gel particles as a function of droplet volume. Uncertainty is expressed as 1σ.

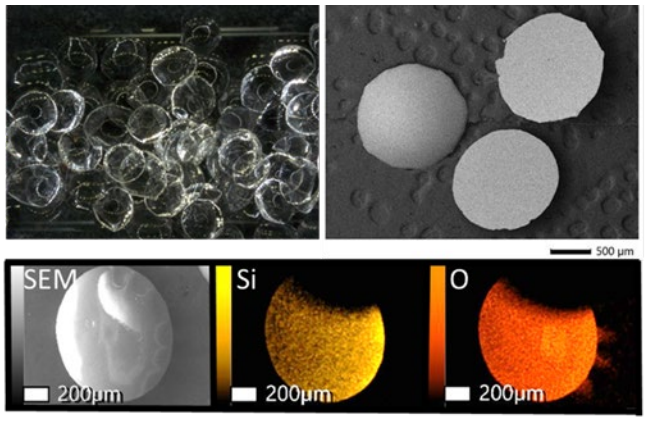

Figure S2. Top left: Microscope image of translucent, non-doped sol-gel particles. Top right: SEM images of non-doped sol-gel particles showing the smooth surface of the top (left particle) and the bottom (right two particles). Bottom: EDS of a non-doped sol-gel particle.

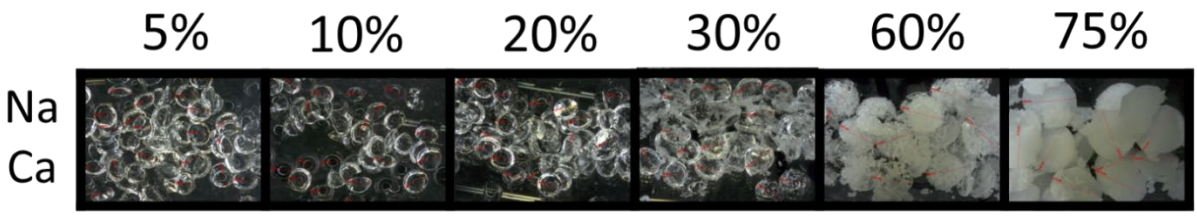

Figure S3. Microscope images of sol-gel particles loaded with Na and Ca nitrates as a function of total metal mol %, with each metal representing an equal portion of the total.

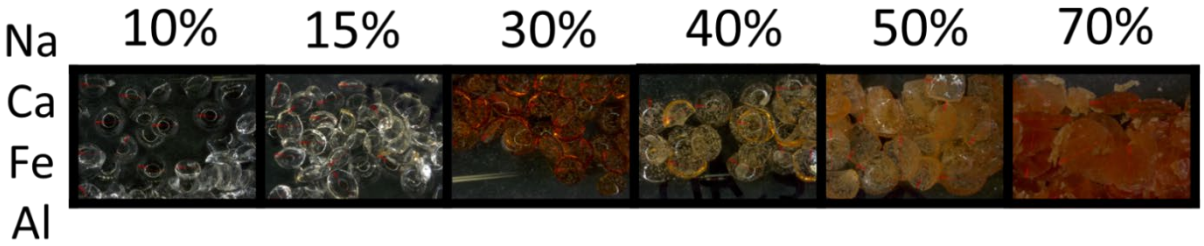

Figure S4. Microscope images showing sol gel particles doped with Na, Ca, Fe, and Al as a function of total metal mol %, with each metal representing an equal portion of the total.

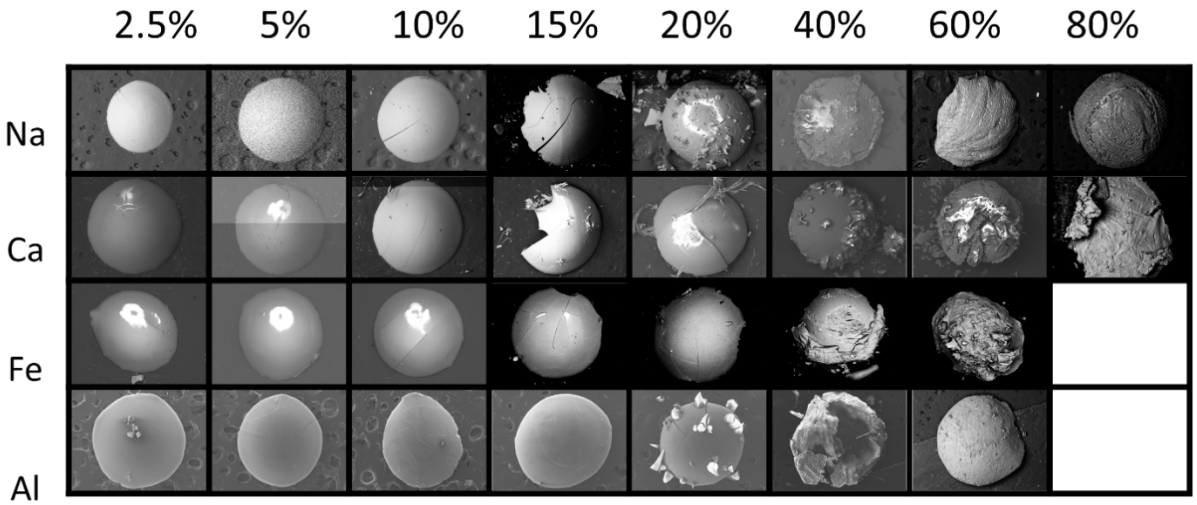

Figure S5. Matrix of metal nitrate loaded sol-gel particle SEM photos as a function of metal mol %.

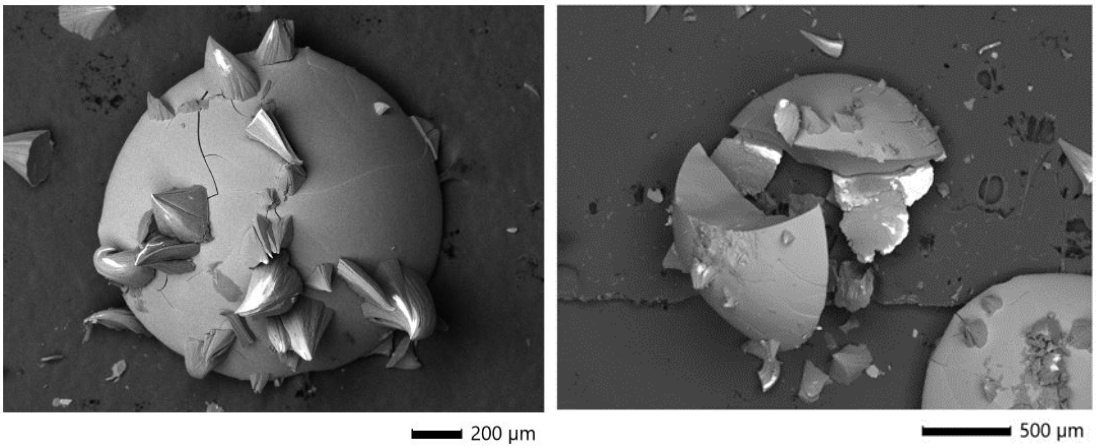

621

622 Figure S6. SEM images of the 20 mol % Al particles that the EDS point analysis reported
623 in Table S1 was done.

624

625 Table S1. EDS point analysis of the 20 mol % Al particles shown in Figure S6.
626 Uncertainty is reported as one standard deviation.

Location	Si (atom %)	O (atom %)	Al (atom %)	N (atom %)
Smooth surface or interior (n=19)	17.0 ± 3.7	67.6 ± 7.8	4.0 ± 0.7	0.0 ± 0.0
Surface feature (n=19)	0.1 ± 0.2	69.3 ± 5.7	7.5 ± 3.1	13.5 ± 3.4

627

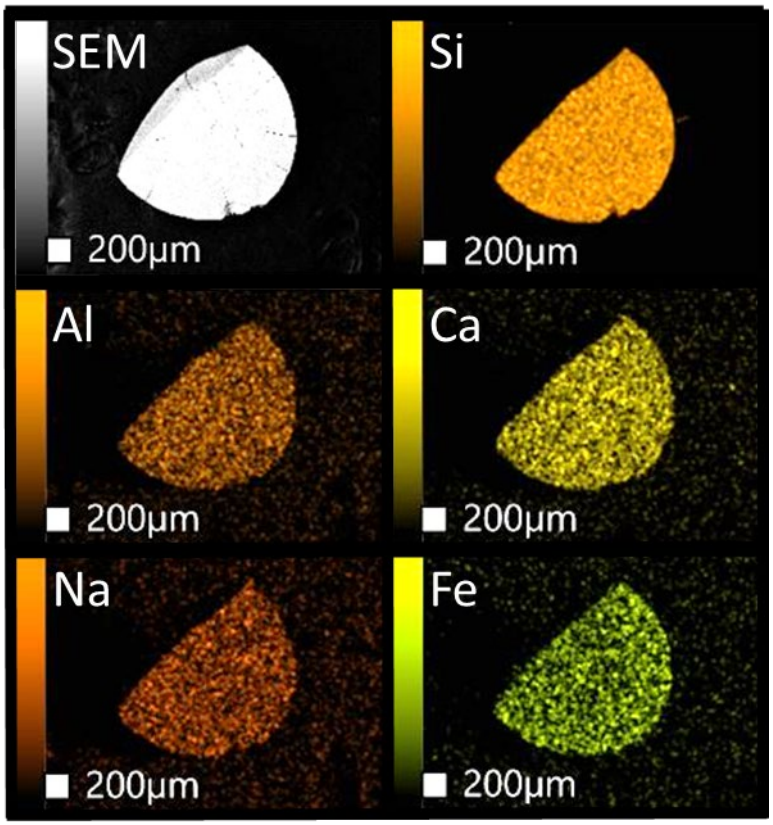

Figure S7. EDS analysis of sol-gel particle doped with Na, Al, Ca, and Fe (20 metal mol % in total).

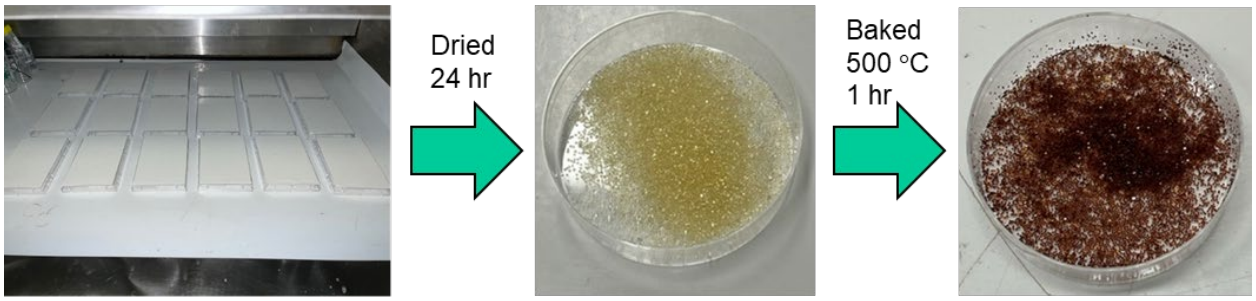

Figure S8. Color change of crustal abundance sample after air drying for 24 hours and then baking for 1 hour at 500ºC.

639

640

641 Table S2. Quantitative results of gamma spectral analysis of NNSS SNED

Isotope	Activity at EOI (Bq)	Unc (1σ)	Estimated Activity at Shipment (Bq)	Unc (1σ)	Number of Effective Fissions at EOI	Unc (1σ)
Tc99m	2.62E+06	1.29E+05	1.28E+06	6.32E+04	1.47E+13	7.53E+11
U237	< MDA		< MDA			
Te132 (Np239)	1.66E+06	7.34E+04	8.97E+05	3.97E+04	1.54E+13	7.20E+11
Np239	3.04E+05	7.68E+03	1.32E+05	3.33E+03		
Ce143	3.11E+06	6.94E+04	7.47E+05	1.67E+04	8.96E+12	2.36E+11
Nd147 (Rh105)	6.93E+06	1.48E+05	5.79E+06	1.24E+05	4.22E+14	1.08E+13
Ru103	9.50E+04	2.34E+03	9.04E+04	2.22E+03	1.53E+13	4.34E+11
Nd147 (I133)	1.57E+05	1.32E+04	1.63E+04	1.37E+03	2.53E+11	2.16E+10
Ba140	3.99E+05	8.99E+03	3.42E+05	7.71E+03	1.02E+13	2.52E+11
Mo99	2.10E+06	5.66E+04	1.03E+06	2.77E+04	1.18E+13	3.58E+11
Zr97	5.52E+06	1.11E+05	3.31E+05	6.67E+03	8.03E+12	2.28E+11
Sr91	7.71E+06	3.45E+05	5.77E+04	2.33E+03	6.62E+12	3.05E+11
Zr95	6.66E+04	1.47E+03	6.46E+04	1.42E+03	8.18E+12	2.14E+11
I132	1.41E+06	3.72E+04	7.66E+05	2.01E+04	1.31E+13	8.39E+12

642

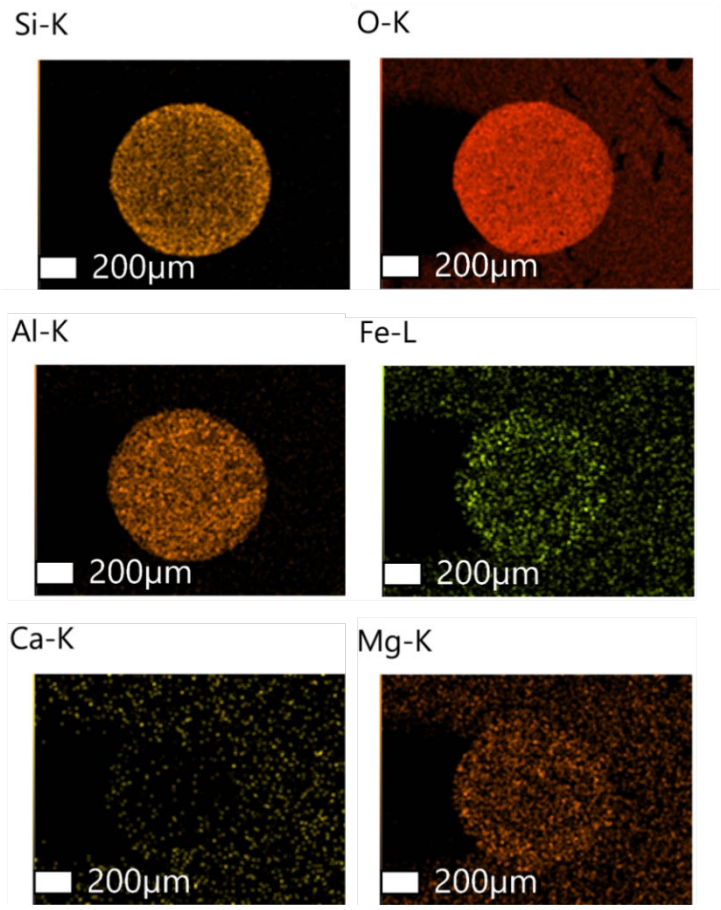

Figure S9. SEM/EDS images of NNSS SNED.